The International Archives of the Photogrammetry, Remote Sensing and Spatial Information Sciences, Volume XLIX-B3-2026
XXV ISPRS Congress 2026 “From Imagery to Understanding”, Commission III, 4–11 July 2026, Toronto, Canada

On the Suitability of Distributed Scatterers for Bridge Monitoring in Very High Resolution SAR Data

Stefan Scheiblauer, Francescopaolo Sica, Michael Schmitt

Department of Aerospace Engineering, University of the Bundeswehr Munich, Neubiberg, Germany - stefan.scheiblauer@unibw.de

Keywords: Persistent Scatterer Interferometry (PSI), Distributed Scatterers (DS), Very High Resolution (VHR) SAR, TerraSAR-X, Bridge Monitoring

Abstract

Satellite-based bridge monitoring with Interferometric Synthetic Aperture Radar (InSAR) offers a cost-effective solution for continuous deformation analysis of critical transport infrastructure. For very high resolution VHR SAR data, distributed scatterers DS suitability for bridge monitoring remains uncertain because elevated decks may suffer layover and partial pixel mixing with underlying terrain. This study evaluates the applicability of DS for bridge monitoring using 23 TerraSAR-X Staring Spotlight over two bridges near Regensburg, Germany: a 930 m long bridge crossing the Danube and agricultural land, and a low overpass crossing the A3 motorway. Persistent Scatterer Interferometry (PSI) was performed with a combined PS/DS workflow, and residual terrain error (RTE) estimates were validated against airborne laser scanning data. The results show that DS can increase measurement density compared with pure persistent scatterers (PS), but their reliability strongly depends on the radiometric contrast between the bridge and its surroundings. For the large bridge over heterogeneous terrain, DS and PS on structural elements yielded physically plausible RTE estimates. In contrast, for the overpass above asphalt surfaces with similar backscatter characteristics, DS were frequently affected by layover between bridge deck and ground, producing large vertical biases, with mean residuals reaching -6.09 m on the carriageway and remaining at -2.12 m even after filtering to above-ground points. The results demonstrate that DS-based bridge monitoring in VHR SAR is feasible where surrounding surfaces are radiometrically distinct; otherwise, DS may lead to erroneous RTE estimation and deformation interpretation.

1. Introduction

Satellite-based bridge monitoring using Interferometric Synthetic Aperture Radar (InSAR) represents a cost-effective approach for continuous deformation measurement. Motorway bridges, as critical infrastructure, are of particular interest (Macchiarulo et al., 2023). Persistent Scatterer Interferometry (PSI) (Ferretti et al., 2001) relies on temporally stable radar reflectors whose phase remains nearly constant over time. These reflectors are typically man-made and are often associated with orthogonal geometries. Because only a limited number of persistent scatterers (PS) are often available, (Ferretti et al., 2011) extended the approach to statistically homogeneous areas, referred to as distributed scatterers (DS). This extension is widely used in ground motion monitoring (Costantini et al., 2021).

For bridge monitoring with very high-resolution (VHR) SAR data, however, it remains unclear whether the DS concept is physically meaningful over elevated bridge decks. Although bridge carriageways may appear homogeneous in SAR amplitude images, side-looking imaging geometry implies that returns from surrounding surfaces, including the ground beneath the bridge, can contribute to the same resolution cell. As a result, DS identified on bridge decks may represent mixtures of signals from different physical surfaces rather than structurally meaningful bridge targets.

In this study, the residual terrain error (RTE) estimated in PSI is used as the primary indicator of physical plausibility, because it reveals whether a selected scatterer is assigned to the bridge elevation or to an alternative effective scattering position. Using two bridge case studies and airborne laser scanning (ALS) data as reference, this work addresses the following questions: (1) under which surface and geometric conditions do DS provide physically plausible RTE estimates on bridges; (2) when do DS over bridge decks become affected by signal mixing and layover; and (3) to what extent do DS increase point density without compromising interpretability.

2. Background

Microwaves are sensitive both to the geometry of the imaged objects and to their surface properties, such as dielectric constant and surface roughness. A surface is considered smooth when its roughness is small compared to the incident radar wavelength λ, as defined by the Fraunhofer criterion (Ulaby and Long, 2014). Figure 1 presents a qualitative comparison: (i) on the left, a smooth surface producing specular reflection with negligible radar return; (ii) in the centre, moderate roughness resulting in a combination of specular and diffuse reflection, leading to a moderate return; and (iii) on the right, a rough surface that generates diffuse scattering.

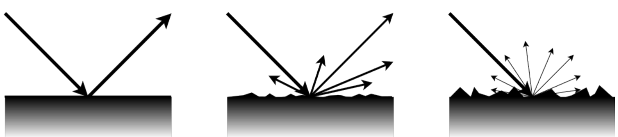

Figure 1. Qualitative illustration of radar scattering across increasing surface roughness: a smooth surface with predominantly specular reflection (left), a moderately rough surface with mixed specular and diffuse reflection (centre), and a rough surface with predominantly diffuse scattering (right).

Distributed scatterer interferometry extends the approach of single temporally phase-stable PS pixels to statistically homogeneous sets of pixels (Ferretti et al., 2011). This is accomplished by means of space-adaptive filters without compromising the information associated with PS points.

By combining surface-dependent backscattering behaviour with the bridge configuration and the underlying terrain, the following considerations arise, as illustrated in Figure 2. The figure depicts the side-looking imaging geometry of spaceborne SAR and the illumination of an elevated bridge cross-section above various surface types. Dashed lines mark the slant-range pixel boundaries.

As shown in Figure 2, contributions to the backscatter over bridges can be attributed to:

- a dominant PS return from the bridge deck and a low or moderate return from the ground,
- specular reflection from the bridge deck and moderate or strong backscattering from the ground,
- comparable contributions from the bridge deck and the surrounding surfaces.

Consequently, in the first case the PS located on the bridge structure dominates the signal. Under the second scenario, if specular reflection occurs on the bridge deck while only low or moderate backscattering originates from the vegetated ground, the total return is weaker and the backscattered signal is primarily attributable to the ground. In the third scenario, in which a bridge crosses a motorway and both carriageways exhibit similar backscatter properties, both surfaces can contribute to the inversion, potentially leading to erroneous RTE estimates and deformation retrievals. If the surface characteristics remain nearly constant over time, the coherence values of layover pixels may exceed the selection threshold. In addition, multipath reflections may occur, producing radar patterns similar to those described by (Soergel et al., 2006).

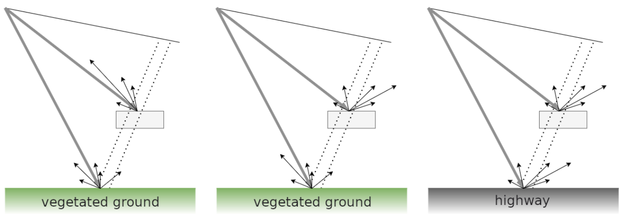

Figure 2. Schematic of backscatter composition for an elevated bridge deck in side-looking SAR geometry. Left: pure Persistent Scatterer (PS) response from the bridge deck. Centre: mixed response from specular deck reflection and moderate contribution from vegetated ground. Right: comparable contributions from both carriageways.

These considerations support pixel differentiation. Unlike buildings, bridges lack continuous radar-facing surfaces and therefore do not exhibit a clear phase ramp. As shown by (Rossi and Eineder, 2015), this phase behaviour helps identify urban structures but does not directly apply to elevated bridge decks.

3. Data and Methods

This study utilises 23 TerraSAR-X Staring Spotlight acquisitions (6 September 2022–25 September 2023) acquired in descending orbit with an incidence angle of 48.75°. This acquisition mode enables the antenna to remain focused on a fixed ground target during the satellite overpass, resulting in an azimuth resolution of up to 25 cm. Furthermore, the 11-day repeat cycle of TerraSAR-X ensures a consistent imaging geometry across all acquisitions, which is a critical requirement for PSI processing. Two assets spanning contrasting surfaces were selected. First, the 930 m long, 47 m high Sinzing A3 motorway bridge crossing the River Danube and agricultural areas near Regensburg, Germany, was analysed. The second asset is a 6.3 m high overpass west of the Danube crossing the A3 motorway with comparable backscatter properties.

Figure 3a presents an overview of the study area in SAR geometry, with the radar line of sight (LOS) oriented from the left. In Figure 3b, stable scatterers aligned along the driving direction of the bridge are identifiable. The area between the bridge decks reveals the ground surface, visible through the field path beneath the structure. Figure 3c shows the overpass oriented perpendicular to the LOS, where multiple reflections occur.

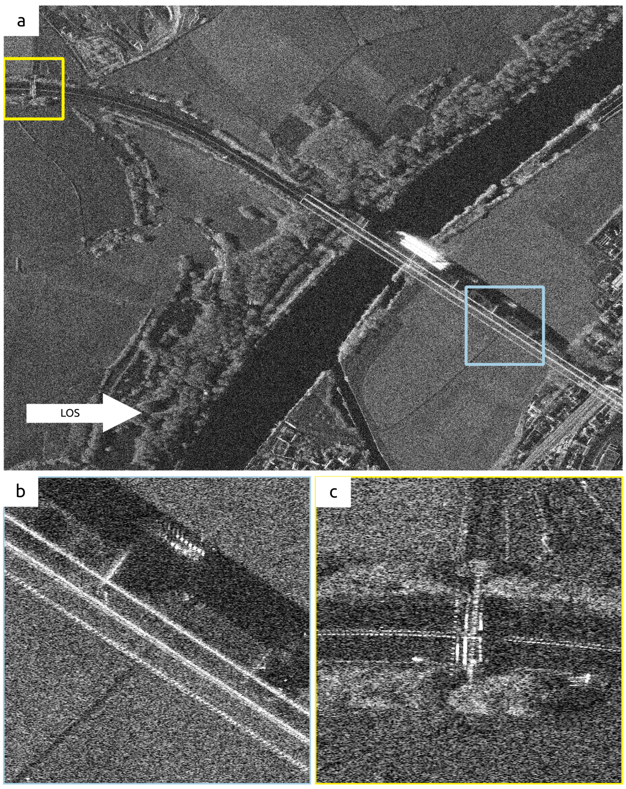

Figure 3. Overview of the A3 Sinzing motorway bridge near Regensburg, Germany, in SAR geometry, acquired on 6 February 2023. SAR illumination is from the left. (a) Overview of the bridge crossing the River Danube and surrounding agricultural land. (b) Detailed view of the motorway bridge, highlighting strong backscatter along the lane margins and weak backscatter from the carriageway, as well as the radar shadow. (c) View of the overpass and multipath reflections adjacent to the structure on the motorway below.

The PSI processing was performed in the commercially avail-

able ENVI® SARscape 6.1.0 (Patch 20250915) software using the combined standard PS and DS workflow. The interferometric network was constructed using a maximum perpendicular baseline threshold of 500 m and a coherence threshold of 0.75. Interferogram generation was assisted by a digital terrain model (DTM). Atmospheric delays were corrected using zenith total delay (ZTD) products provided by the Generic Atmospheric Correction Online Service for Interferometric Synthetic Aperture Radar (GACOS) (Yu et al., 2018). Statistically homogeneous pixels were identified in the adaptive filtering stage using the Kolmogorov–Smirnov test within a 5×5 window at a significance level of 0.05. In the first inversion step, RTE and linear deformation velocity were estimated for each scatterer, whereas in the second step the atmospheric phase screen was refined to improve the displacement time series. The final products, including RTE estimates and acquisition-wise displacement estimates, were exported in geospatial vector format for subsequent analysis.
A buffer of 1 m was applied around the line displayed in Figures 4 and 5 to select PS and DS points for evaluation. To investigate the agreement between PS/DS locations and structural bridge elements, the ALS data were divided into subsets (Table 1). The results are compared with airborne laser scanning data provided by the Bavarian State Agency for Digitisation, High-Speed Internet and Surveying (Landesamt für Digitalisierung, Breitband und Vermessung (LDBV) Bayern, 2025). For the motorway bridge, the analysis was subdivided into western, central, and eastern sections. The western and eastern sections represent the bridge edges, including guardrails and other elevated structures, whereas the central section represents the carriageway separator. For the comparison, the datasets for the bridge and the overpass were split into pure PS points and distributed scatterers and further divided into spatial clusters to evaluate the performance with respect to the ALS data serving as reference.
For each subset, point-wise vertical residuals were computed as

$$r_i = z_i^{\mathrm{RTE}} - \bar{z}_{\mathrm{ALS}}, \tag{1}$$

where z_i^{RTE} denotes the RTE and $\bar{z}_{\mathrm{ALS}}$ the corresponding arithmetic mean of the ALS reference elevations.

Based on these residuals, the following parameters were calculated:

- *Number of PSI points* (N): number of PS or DS points contained in the evaluated subset.
- *Mean RTE* ($\bar{z}_{\mathrm{RTE}}$): arithmetic mean of the scatterer elevations reconstructed from the RTE estimates.
- *Mean residual* ($\bar{r}$): arithmetic mean of the residuals,

$$\bar{r} = \frac{1}{N}\sum_{i=1}^{N} r_i, \tag{2}$$

which is equivalent to the bias and indicates systematic overestimation ($\bar{r} > 0$) or underestimation ($\bar{r} < 0$) of RTE relative to the ALS reference.

- *Root-mean-square error* (RMSE): defined as

$$\mathrm{RMSE} = \sqrt{\frac{1}{N}\sum_{i=1}^{N} r_i^2}, \tag{3}$$

providing an aggregate measure of total vertical error magnitude.

- *Standard deviation* (σ_r): sample standard deviation of the residuals,

$$\sigma_r = \sqrt{\frac{1}{N-1}\sum_{i=1}^{N} (r_i - \bar{r})^2}, \tag{4}$$

representing the spread of the residual distribution.

- *Median residual*: 50th percentile of the residual distribution, providing a robust measure of central tendency.
- *Mean absolute error* (MAE): defined as

$$\mathrm{MAE} = \frac{1}{N}\sum_{i=1}^{N} |r_i|, \tag{5}$$

These metrics were used to assess the absolute vertical agreement of PS and DS solutions with the reference data and to compare performance across infrastructure type and spatial cluster.

4. Results

We show results in Table 1 and summarise the comparison between the ALS reference elevations and the elevations reconstructed from the PSI-derived RTE. All heights are reported as ellipsoidal heights. The evaluation subsets are indicated by the grey boxes in Figures 4 and 5. Overall, the number of PS points was very limited in all selected cross-sections. As shown in Figure 4, only five PS points were identified on the motorway bridge in total. Mean residuals range from -2.175 m in the western section to -0.026 m in the eastern section. The central bridge section contained a single PS point with a residual of -0.389 m. For the overpass (Figure 5), six PS points were detected, yielding positive mean residuals of 0.408 m and 0.858 m for the western and eastern edges, respectively.
In contrast, DS points were substantially more abundant than PS points in all subsets. For the motorway bridge, 118 DS points were identified in total. The DS mean residuals show a clear spatial gradient, increasing from -3.465 m in the western section to -0.405 m in the central section and to 0.309 m in the eastern section. The same trend is reflected by the median residuals, which increase from -3.241 m to -0.496 m and 0.415 m, respectively. The western bridge edge also exhibits the largest bridge-related DS error metrics, with an RMSE of 3.550 m and a residual standard deviation of 0.780 m.
A comparable behaviour is observed for the overpass. Only two DS points were detected at the eastern edge (Table 1), with a mean residual of 1.014 m. On the carriageway, however, 185 DS points were identified, indicating that the overpass surface was represented mainly by distributed rather than persistent scatterers (Figure 5). For the unfiltered carriageway subset, the residuals are strongly biased towards lower elevations, with a mean residual of -6.086 m, a median of -8.245 m, and a standard deviation of 3.486 m. After restricting the analysis to points above ground level, the above-ground subset retains 76 DS points and shows markedly improved agreement with the ALS data, with the mean residual reduced to -2.117 m, the median to -2.042 m, and the standard deviation to 1.175 m. The motorway subset east of the overpass contains 162 DS points, with a mean residual of 3.445 m, an RMSE of 3.717 m, a residual standard deviation of 1.400 m, and a median of 3.185 m.

Asset	Subset	Scatterer	N	$\bar{z}_{\mathrm{ALS}}$	$\bar{z}_{\mathrm{RTE}}$	$\bar{r}$	$RMSE$	Std. σ_r	$Median$	MAE
Bridge	West	PS	3	424.380	422.205	-2.175	2.184	0.239	-2.173	2.175
	Centre	PS	1	424.418	424.029	-0.389	0.389	—	-0.389	0.389
	East	PS	1	424.580	424.554	-0.026	0.026	—	-0.026	0.026
	West	DS	52	424.380	420.914	-3.465	3.550	0.780	-3.241	3.465
	Carriageway West	DS	18	424.205	421.834	-2.371	2.855	1.637	-2.626	2.371
	Centre	DS	44	424.418	424.013	-0.405	0.645	0.507	-0.496	0.553
	Carriageway East	DS	20	424.157	424.983	0.826	0.951	0.485	0.956	0.837
	East	DS	22	424.580	424.888	0.309	0.519	0.427	0.415	0.439
Overpass	West	PS	1	454.225	454.633	0.408	0.408	—	0.408	0.408
	East	PS	5	454.203	455.061	0.858	0.948	0.452	0.924	0.858
	East	DS	2	454.203	455.217	1.014	1.167	0.817	1.014	1.014
	Carriageway	DS	185	452.937	446.851	-6.086	7.009	3.486	-8.245	6.094
	Above-ground	DS	76	452.937	450.820	-2.117	2.418	1.175	-2.042	2.136
	Motorway	DS	162	447.316	450.761	3.445	3.717	1.400	3.185	3.490

Table 1. Statistical comparison of point scatterers (PS) and distributed scatterers (DS) for the evaluated bridge and overpass subsets. For each asset subset and scatterer class, the table reports the number of retained scatterers (N), the mean ALS reference elevation ($\bar{z}_{\mathrm{ALS}}$), the mean RTE ($\bar{z}_{\mathrm{RTE}}$), the mean residual ($\bar{r}$), the root-mean-square error (RMSE), the sample standard deviation of the residuals (σ_r), the median residual, and the mean absolute error (MAE). Positive residuals indicate RTE overestimation relative to the ALS reference, while negative residuals indicate underestimation.

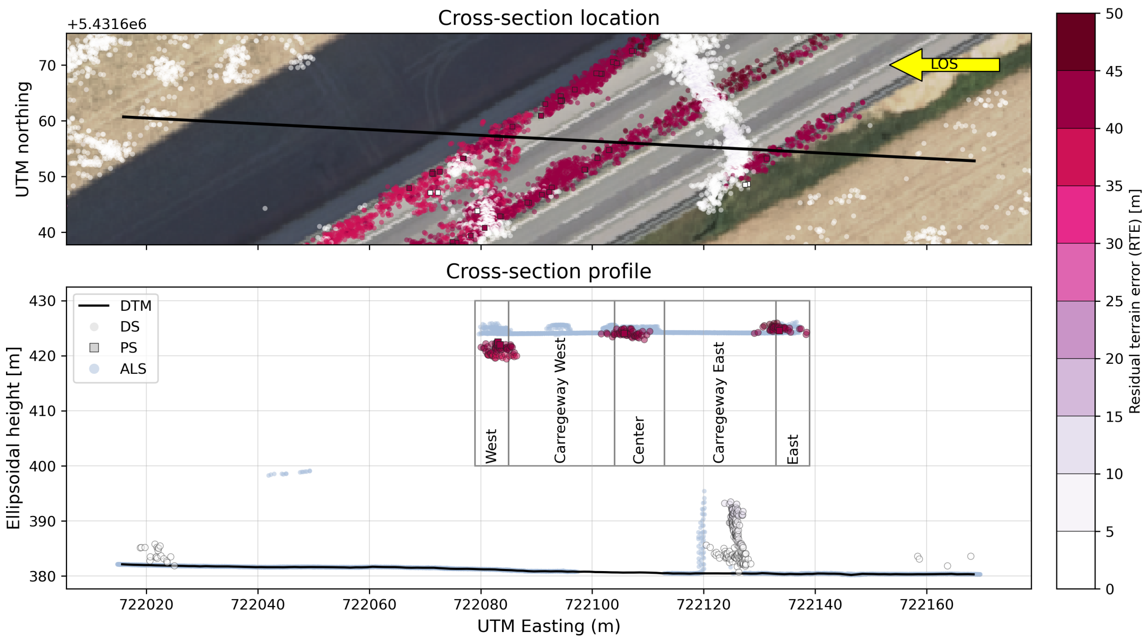

Figure 4. Cross-section of the A3 motorway bridge near pier 4. Top: residual terrain error (RTE, m); circles denote distributed scatterers (DS), squares persistent scatterers (PS), and the black line the selected cross-section. Bottom: ellipsoidal height profile; the black line denotes the DTM, the points the scatterer elevations reconstructed from the estimated RTE, and the bluish circles the ALS reference data.

5. Discussion

The motorway bridge crossing the River Danube shown in Figure 4 indicates that pronounced radiometric contrast between bridge elements and the surrounding surfaces is the main factor enabling a physically meaningful estimation of the RTE. Where bridge-related structures can be distinguished clearly from ground-related contributions, the resulting scatterers are more likely to represent elevated structural elements rather than mixed responses from different surfaces. By contrast, the overpass example in Figure 5 highlights a more general limitation of DS under layover conditions in VHR SAR data. When the overpass carriageway and adjacent surfaces exhibit similar backscatter behaviour, statistically similar pixels may be grouped into a common DS patch even though they originate from physically distinct structures. In such cases, the estimated RTE no longer represents a single, well-defined surface, but rather a mixed response influenced by the local imaging geometry.

The comparison of the overpass subsets suggests that the observed errors arise from i) layover and ii) a combination of layover contributions and multipath effects. The evaluated motorway subset east of the overpass (Figure 5) provides an important reference, because all analysed points are located above ground. In this motorway section, the mean residual is 3.445 m, which is approximately half the vertical separation between the motorway and the overpass carriageway. This behaviour is consistent

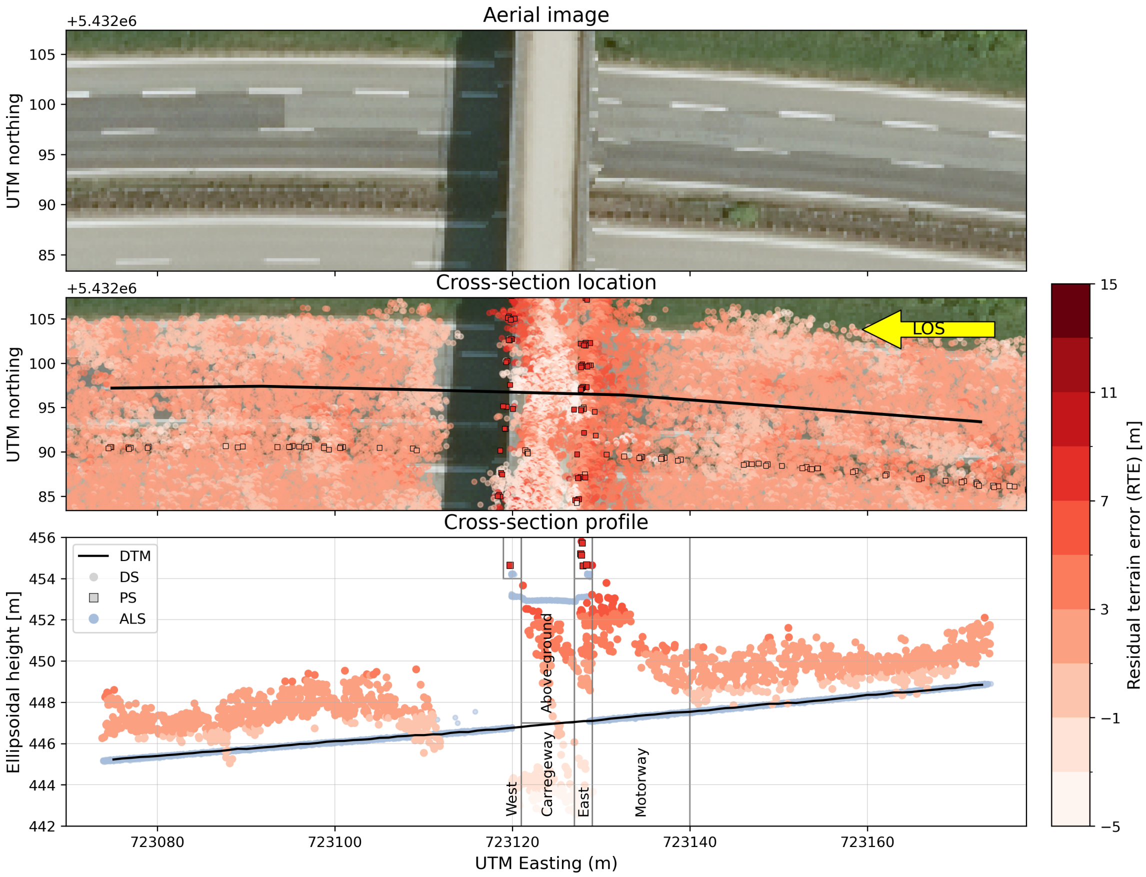

Figure 5. Cross-section of the A3 motorway overpass near Regensburg. Top: aerial image of the overpass. Middle: residual terrain error (RTE, m); circles denote distributed scatterers (DS), squares persistent scatterers (PS), and the black line the selected cross-section. Bottom: ellipsoidal height profile; the black line denotes the DTM, the points the scatterer elevations reconstructed from the estimated RTE, and the bluish circles the ALS reference data.

with range resolution cells containing contributions from both the motorway and the overpass carriageway, which are then represented by a single DS despite originating from different physical structures. As a result, the derived RTE is displaced from the true location of either surface and becomes physically ambiguous. For the carriageway subset of the overpass, this effect is further compounded by multipath. In addition to the mixed backscatter from spatially distinct surfaces, the signal is likely additionally affected by an increased propagation path caused by interactions between the built structure and its surroundings. This provides a plausible explanation for the strongly negative residuals observed for the unfiltered carriageway subset, where the mean residual reaches -6.086 m. The above-ground filtered subset reduces this effect, but the remaining residuals still indicate that part of the DS population does not correspond exclusively to the bridge deck.

6. Conclusion

The contrast between the motorway bridge and the overpass therefore underlines that DS-based RTE estimation in VHR SAR data depends strongly on local scene structure and radiometric separability. Where the bridge geometry produces distinct backscatter signatures, DS can provide spatially meaningful estimates. Where layover combines surfaces with similar scattering characteristics, DS may represent physically separated structures and yield erroneous elevations. However, the separation of such overlaid signals may still be feasible with more advanced approaches. In particular, SAR Tomography has been shown to separate PS contributions in urban settings (Zhu and Bamler, 2010). From an application perspective, DS-based bridge monitoring in VHR SAR should therefore include a priori screening of local backscatter characteristics and imaging geometry. In low-contrast layover configurations, DS-based RTE estimates should be screened carefully and excluded where necessary, even at the expense of reduced point density.

References

Costantini, M., Minati, F., Trillo, F., Ferretti, A., Novali, F., Passera, E., Dehls, J., Larsen, Y., Marinkovic, P., Eineder, M., Brcic, R., Siegmund, R., Kotzerke, P., Probeck, M., Kenyeres, A., Proietti, S., Solari, L., Andersen, H. S., 2021. European Ground Motion Service (EGMS). *Proceedings of IEEE International Geoscience and Remote Sensing Symposium*, 3293–3296.

Ferretti, A., Fumagalli, A., Novali, F., Prati, C., Rocca, F., Rucci, A., 2011. A New Algorithm for Processing Interferometric Data-Stacks: SqueeSAR. *IEEE Transactions on Geoscience and Remote Sensing*, 49(9), 3460–3470.

Ferretti, A., Prati, C., Rocca, F., 2001. Permanent scatterers in SAR interferometry. *IEEE Transactions on Geoscience and Remote Sensing*, 39(1), 8–20.

Landesamt für Digitalisierung, Breitband und Vermessung (LDBV) Bayern, 2025. Digitales Geländemodell 1m (DGM1).

Macchiarulo, V., Milillo, P., Blenkinsopp, C., Reale, C., Giardina, G., 2023. Multi-temporal InSAR for transport infrastructure monitoring: recent trends and challenges. *Proceedings of the Institution of Civil Engineers - Bridge Engineering*, 176(2), 92–117.

Rossi, C., Eineder, M., 2015. High-Resolution InSAR Building Layovers Detection and Exploitation. *IEEE Transactions on Geoscience and Remote Sensing*, 53(12), 6457–6468.

Soergel, U., Gross, H., Thiele, A., Thoennessen, U., 2006. Extraction of bridges over water in multi-aspect high-resolution InSAR data. *International Archives of the Photogrammetry, Remote Sensing and Spatial Information Sciences*, 36(Part 3), 185–190.

Ulaby, F. T., Long, D. G., 2014. *Microwave radar and radiometric remote sensing*. University of Michigan press, Ann Arbor.

Yu, C., Li, Z., Penna, N., Crippa, P., 2018. Generic atmospheric correction online service for InSAR (GACOS). *EGU General Assembly Conference Abstracts*, 11007.

Zhu, X. X., Bamler, R., 2010. Very High Resolution Spaceborne SAR Tomography in Urban Environment. *IEEE Transactions on Geoscience and Remote Sensing*, 48(12), 4296–4308.

https://doi.org/10.5194/isprs-archives-XLIX-B3-2026-523-2026